Magnetic order in XY-type antiferromagnetic monolayer $CoPS_3$ revealed by Raman spectroscopy

Qiye Liu,[1,2,*] Le Wang,[1,*] Ying Fu,[1] Xi Zhang,[5] Lianglong Huang,[1] Huimin Su,[1] Junhao Lin,[1] Xiaobin Chen,[6] Dapeng Yu,[1] Xiaodong Cui,[2] Jia-Wei Mei,[1,4,†] and Jun-Feng Dai[1,3,†]

[1]*Shenzhen Institute for Quantum Science and Engineering, and Department of Physics, Southern University of Science and Technology, Shenzhen 518055, China*

[2]*Department of Physics, The University of Hong Kong, Pokfulam 999077, Hong Kong*

[3]*Shenzhen Key Laboratory of Quantum Science and Engineering, Shenzhen 518055, China*

[4]*Shenzhen Key Laboratory of Advanced Quantum Functional Materials and Devices, Southern University of Science and Technology, Shenzhen 518055, China*

[5]*Shannxi Institute of Flexible Electronics, Northwestern Polytechnical University, Xi'an 710072, China*

[6]*School of Science and State Key Laboratory on Tunable Laser Technology and Ministry of Industry and Information Technology Key Lab of Micro-Nano Optoelectronic Information System, Harbin Institute of Technology, Shenzhen 518055, China*

(Received 19 March 2021; revised 20 May 2021; accepted 24 May 2021; published 7 June 2021)

Mermin-Wagner-Coleman theorem predicts no long-range magnetic order at finite temperature in the two-dimensional (2D) isotropic systems, but it does predict a quasi-long-range order with a divergent correlation length at the Kosterlitz-Thouless (KT) transition for planar magnets. As a representative of two-dimensional planar antiferromagnets, single-layer $CoPS_3$ carries the promise of monolayer antiferromagnetic platforms for the ultimately thin spintronics. Here, with the aid of magnetostriction which is sensitive to the local magnetic order, we observe the signature phonon mode splitting of below T_{KT} in monolayer $CoPS_3$. The two-magnon signal in the monolayer one manifests the associated magnetic transition. It indicates the quasi-long-range order in an exact 2D planar spin model below KT phase transition. The ratio (J'/J) between the interlayer and intralayer interactions, which characterizes the 2D behaviors, is evaluated to be around 0.03. Our results provide an efficient method to detect the quasi-long-range antiferromagnetic ordering in the two-dimensional magnets down to the monolayer limit.

DOI: 10.1103/PhysRevB.103.235411

I. INTRODUCTION

As the scale of conventional ferromagnetic storage devices is approaching the limit of the critical domain size, growing interest has be concentrated on magnetic materials down to single atomic layer for high-density information storage and spintronic devices. It makes the two-dimensional (2D) ferromagnetic materials a present hot spot along this approach [1–11]. Besides the ferromagnetic materials, antiferromagnetic materials play a unique role in spintronic devices thanks to the robustness of antiferromagnetic order to resist sizable external interference and zero net magnetization without any stray field [12]. Fundamentally both ferromagnetic and antiferromagnetic magnets are addressed in the similar frame of magnetic ordering. For Ising-type magnets where spin points in one direction either up or down [13], the phase transition is demonstrated experimentally in monolayer ferromagnet $Cr_2Ge_2Te_6$ [1] and CrI_3 [2] by magneto-optical Kerr effect (MOKE). The 2D XY-type system with spin confining within the *a-b* plane is quite different from the Ising type as the Mermin-Wagner-Coleman theorem states that the long-range magnetic orders are suppressed at finite temperature [14,15]. Instead, the 2D XY-type magnetic materials could also be materialized in quasi-long-range magnetic ordered 2D systems. There is a presence of a phase transition at finite temperature to a phase without long-range order, but with a diverging in-plane correlation length. Such a phase transition is called the Kosterlitz-Thouless (KT) transition in 2D systems [16], which corresponds to a gas of free vortices into binding of vortex-antivortex pairs at a temperature T_{KT}. This diverging correlation length could lead to a quasi-long-range magnetic ordering and consequently a 2D magnet.

The emergence of transition metal phosphorus trisulfides (MPS_3, M = Mn, Fe, Co, Ni) [17–19], which is a class of potential 2D van der Waals (vdW) magnetic materials [Fig. 1(a)] provides a platform to explore the magnetic ordering down to the monolayer limit. In contrast to $FePS_3$ and (Mn/Ni)PS_3 which are recognized as Ising-type and Heisenberg-type antiferromagnets in bulk form [20–24], respectively, $CoPS_3$ is one of 2D XXZ antiferromagnets [25]. Mn^{2+} and Ni^{2+} have the electronic configurations $3d^5$ and $3d^8$, respectively, in which the orbital degree of freedom for the d electrons is quenched. The spin-orbit coupling is negligible, and then (Mn/Ni)PS_3 are the almost isotropic Heisenberg-type antiferromagnets. Fe^{2+} and Co^{2+} have the electronic configurations $3d^6$ and $3d^7$, respectively, and the orbital degree is partially quenched. The spin-orbit coupling between spins and the unquenched orbitals accounts

*These authors contributed equally to this work.
†Corresponding authors: meijw@sustech.edu.cn; daijf@sustech.edu.cn

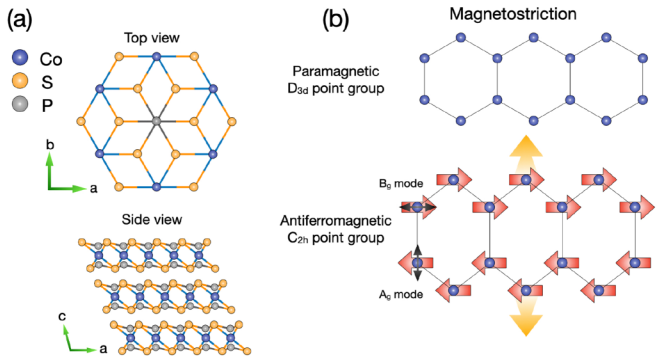

FIG. 1. (a) Top view of monolayer $CoPS_3$ and side view of crystal structure of bulk $CoPS_3$. Blue, orange, and gray balls represent Co, S, and P atoms, respectively. (b) Magnetostriction in monolayer $CoPS_3$, where a structural distortion is induced at antiferromagnetic state. In this case, it belongs to C_{2h} point group. At paramagnetic state, crystal structure is close to being orthohexagonal and is described by D_{3d} point group. Red arrows represent the spin orientations of Co atoms at antiferromagnetic state and orange ones represent extension of lattice structure. A_g and B_g vibration modes are also indicated by the black arrows, which are parallel and perpendicular to spin orientation, respectively.

for the magnetic anisotropies in $FePS_3$ and $CoPS_3$, resulting in the Ising-type and XXZ-type antiferromagnets, respectively. The monolayer $CoPS_3$ as an exact 2D planar spin model likely exhibits the magnetic KT transition, however, experimental demonstration of the quasi-long-range order is challenging.

The spin-orbit coupling in $FePS_3$ and $CoPS_3$ due to the unquenched orbitals induces the structural change of magnetic materials under a magnetic phase transition, i.e., the magnetostrictive effect [26,27], which can be used as a predominant indicator of magnetic phase. For bulk $FePS_3$, the magnetostriction has been systematically studied by the low-temperature x-ray diffraction and neutron scatterings [28,29]. At the antiferromagnetic transition temperature in $FePS_3$, the lattice parameter c still linearly decreases continuously, whereas parameters a and b remarkably change in the opposite way, where the a axis shrinks and b axis extends, respectively [Fig. 1(b)]. This indicates that the magnetostriction of $CoPS_3$ can be used to probe the magnetic transition. Moreover, since it depends only on the local correlation, the magnetostriction should be sensitive to the quasi-long-range ordering even down to the monolayer limit. Along this line, in this work, we monitor the structural change by the Raman spectroscopy to probe the associated magnetic KT transition in single- and few-layered $CoPS_3$. The structural change is characterized by the phonon mode splitting of Co-atom related vibration in Raman spectra, and the phase transition temperature T_{KT} is observed to be $\sim$100 K for the thin $CoPS_3$ from monolayer to quadlayer, lower than the bulk antiferromagnetic transition temperature $T_N = 118$ K. The associated magnetic transition in the monolayer $CoPS_3$ is also identified by the two-magnon signal. Our work demonstrates the implementation of magnetostrictive effect in the exact 2D magnetic materials for the probe of the quasi-long-range order below the KT transition.

II. EXPERIMENTAL METHODS

High quality $CoPS_3$ single crystals were grown by the chemical vapor transport (CVT) method and characterized with x-ray diffraction (see Fig. S1 of the Supplemental Material [30]) and x-ray photoemission (Fig. S2 [30]) techniques. The magnetic susceptibility (χ) [Fig. S3(a)] and specific heat [Fig. S3(b)] measurements in $CoPS_3$ single crystal reveal a magnetic phase transition from paramagnetic to antiferromagnetic states at $\sim$118 K as reported by Wildes *et al.* [30,31]. Recent neutron diffraction [31] studies have revealed that $CoPS_3$ has an intralayer antiferromagnetic structure, where ferromagnetic "zigzag" chains are formed along the a axis, while adjacent chains are coupled antiparallelly along the b axis [Fig. 1(b)]. As shown in Fig. 1(a), monolayer $CoPS_3$ has a hexagonal structure for moments on Co^{2+} irons; for few layered $CoPS_3$, adjacent layers are weakly coupled to each other by vdW forces along the c axis. Therefore, $CoPS_3$ flakes can be mechanically exfoliated from single crystal onto SiO_2/Si substrates using sticky tape in a glove box filled with nitrogen [30], which is a common method to produce transition metal dichalcogenide (TMDC) sheets [32,33]. The optical and atomic force microscope (AFM) images of monolayer $CoPS_3$ is shown in Fig. 2(a). The thickness of monolayer $CoPS_3$ is around 0.80 nm. In addition, the thickness of bilayer, trilayer, and quadlayer $CoPS_3$ is 1.49, 2.26, and 2.86 nm (Fig. S4 [30]), respectively.

The polarized Raman spectroscopy [34,35] has been proved to be sensitive to a structural change even for atomically thin samples. Hence, in this study, we apply the polarized Raman spectroscopy to characterize the magnetic state and crystal structural change in monolayer $CoPS_3$. The schematic of polarization-resolved Raman measurement is shown in Fig. S5 and more details about measurements can be found in the Supplemental Material [30]. Figure 2(b) shows the representative circularly polarized Raman spectra of a monolayer $CoPS_3$ at room temperature ($T = 295$ K) and low temperature ($T = 25$ K). Here we excite the samples with a left-handed (L) circularly polarized light, and monitor the left-handed (L) and right-handed (R) circularly polarized components of Raman signals.

III. RESULTS AND DISCUSSIONS

Five unambiguous peaks are clearly identified at room temperature. Based on D_{3d} point group, two modes at around 149 (P_2) and 278 (P_6) cm^{-1} are assigned to the double-degenerate E_g modes, whereas three peaks at around 242 (P_5), 384 (P_7), and 585 (P_9) cm^{-1} are nondegenerate A_g vibration modes. With the aid of density-functional theory (DFT) calculations (Table S1 [30]), the low-frequency peak (P_2) is attributed to in-plane Co-atom related vibrations, while P_5, P_6, and P_7 modes originate from out-of-plane and in-plane vibrations of S-S atoms and P_9 is the out-of-plane vibrations of P-P atoms. Other Raman peaks listed in the Table S1, including P_1, P_4, and P_8, cannot be detected in monolayer $CoPS_3$ due to relatively weak signal strength. While for bulk $CoPS_3$, these three peaks centered at around 111 (P_1), 229 (P_4), and 559 (P_8) cm^{-1} can be clearly resolved [Fig. 2(c)], which are assigned as double-degenerate E_g modes. Among them, P_1 is also

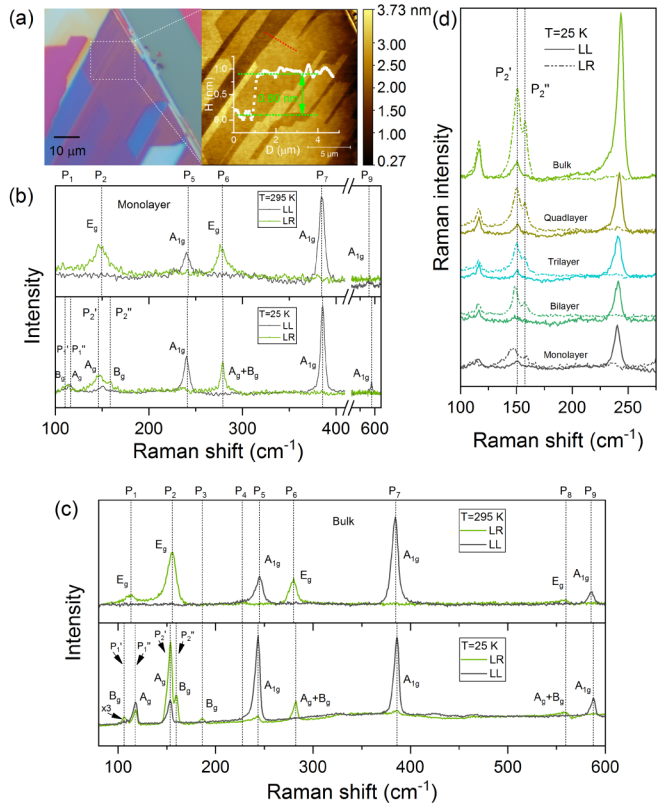

FIG. 2. (a) Optical and AFM image of monolayer $CoPS_3$. The height of the monolayer $CoPS_3$ is about 0.80 nm and the sample size is larger than 10×10 μm. Circularly polarized Raman spectra of the monolayer (b) and bulk (c) $CoPS_3$ measured at 295 and 25 K in circularly copolarization (LL) and cross-polarization (LR) scattering configurations, respectively. LL (LR): the first letter represents the polarized state of excited light, whereas the second letter represents the polarized state of scattering Raman signal. L and R means left-handed and right-handed circularly polarized light, respectively. The dashed lines indicate the position of peaks, labeled as P_1 to P_9. The corresponding Ramon modes are summarized in Table S1 and shown in the figure. Compared with the spectra at 295 K, P_2 peak splits into two components at low temperature, labeled as P_2' and P_2''. (d) Raman spectra of $CoPS_3$ with different layer numbers in LL (dashed lines) and LR (solid lines) configurations at 25 K, respectively. The splitting of P_2 peak still can be observed in all the samples as indicated by two dashed lines.

related to in-plane Co-atom related vibrations. In addition, P_3 corresponds to the nonactive A_{2g} mode in the D_{3d} point group at room temperature. These findings are consistent with the results in the literature [36], which also implies the high quality of our experimental samples.

At low temperature, a remarkable change can be found at the phonon peak P_2, where the double-degenerate E_g mode at around 149 (P_2) cm^{-1} at 295 K splits into two components with peak positions at around 146 (P_2') and 158 (P_2'') cm^{-1} at 25 K in the circularly cross-polarized (LR) component of Raman spectrum, respectively. The changes of the peak position of P_2' and P_2'' show opposite trends with respect to the P_2 peak, i.e., redshift for P_2' and blueshift for P_2''. Meanwhile there is no noticeable splitting in another E_g mode (peak P_6) corresponding to the in-plane vibrations of S-S atoms. In addition, a new peak centered at around 146 (P_2') cm^{-1} appears in the copolarized (LL) component of Raman spectrum, which is absent in the corresponding spectrum at 295 K. The similar peak splitting can also be observed in the P_1 peak in bulk $CoPS_3$ [Fig. 2(c)], which is also corresponding to the Co-atom related vibration mode. For bilayer, trilayer, quadlayer, and even bulk $CoPS_3$, the P_2 peak splitting is clearly observed as indicated by the dashed lines in Fig. 2(d). The corresponding Raman signals (P_2') in circularly copolarized (LL) component gradually rise with the increasing number of layers. Moreover, for the P_5 and P_7 peaks in bulk $CoPS_3$ [Fig. 2(c)], an extra component of LR configuration emerges in the Raman spectra at 25 K, while a new peak centered at around 187 cm^{-1} (P_3) also appears in LR configuration at 25 K.

According to Raman tensor analysis [30], the structure of monolayer $CoPS_3$ is orthohexagonal at high temperature, and the Raman-active phonon modes can be described as the point group D_{3d}. At low temperature, the double degenerate E_g mode tends to split into A_g and B_g modes. While the A_{1g} mode turns to be an A_g, which responds differently from that emerged from the E_g mode. The invisible A_{2g} mode turns to be a B_g mode. The symmetry analysis of the mode evolution from high temperature to low temperature implies that the Raman tensors shifts from the point group D_{3d} to C_{2h} due to the structural distortion in monolayer $CoPS_3$ system [34], as illustrated in Fig. 1(b). Based on the Raman tensors of the C_{2h} point group [30] we except that for the B_g mode, the left-handed circularly polarized excitation generates the right-handed circularly polarized Raman signal, or vice versa, whereas the A_g mode will appear in both components, i.e., the left-handed and right-handed components, under a left-handed (or right-handed) circularly polarized excitation. These are consistent with our experimental observation. Following this rule, the P_2' (P_1'') is assigned as an A_g phonon mode, while the P_2'' (P_1') belongs to a B_g phonon mode at low temperature. The layer-independent peak splitting [Fig. 2(d)] also indicates that intralayer structural distortion dominates the Raman response instead of the tiny interlayer translation.

To further confirm that the peak splitting or the structural distortion is related to magnetic behaviors in the monolayer limit, we also inspect the linearly polarized Raman spectra as a function of temperature in the monolayer $CoPS_3$. In this case, the P_2' and P_2'' will emerge at cross-polarization (XY) and copolarization (XX) scattering configurations, respectively, so that we can exactly extract the peak position at different temperatures. As shown in Fig. 3(a), we can clearly see that the split doubly degenerated P_2 peaks gradually merge into one peak with increasing temperature. The frequency difference ($\Delta P_2 = P_2'' - P_2'$) between two split peaks [black squares in Fig. 3(b)] remains above 8 cm^{-1} below ~56 K. After that, it dramatically decreases and approaches zero above ~100 K. The similar peak splitting near 154 cm^{-1} and its temperature dependence are also observed in another monolayer $CoPS_3$ (sample 2) (Fig. S7 [30]). The energy shift of the P_2 peak in two monolayer samples may originate from various substrate-induced strains. In addition, Fig. 3(b) also shows that the splitting of the P_2 for samples of bi-, tri-, and quadlayers exhibits similar temperature dependence to that of the monolayer one with the same transition temperature of

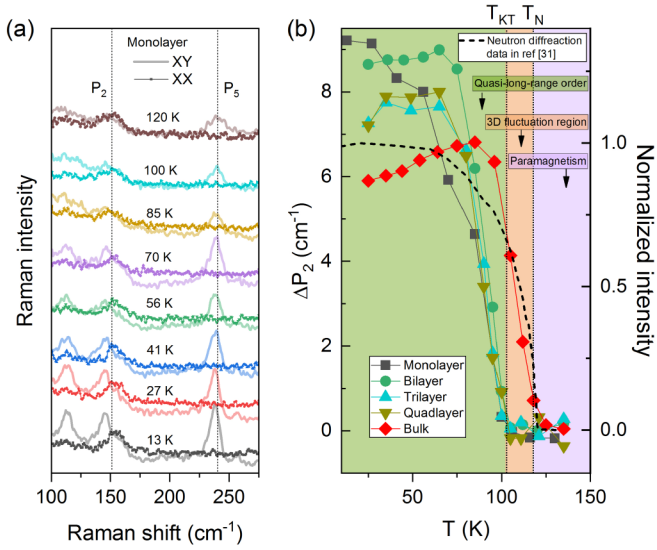

FIG. 3. (a) Raman spectra of monolayer $CoPS_3$ at several representative temperatures in copolarization (XX) (dashed lines) and cross-polarization (XY) (solid lines) configurations, respectively. The dashed lines indicate the peak position of P_2 and P_5 at room temperature. (b) ΔP_2 as a function of temperature in $CoPS_3$ with different layer numbers and neutron diffraction data in Ref. [31]. The dashed line indicates the position of T_{KT} and T_N, respectively. Three regions are filled with different colors and labeled as quasi-long-range order, 3D fluctuation region, and paramagnetism, respectively.

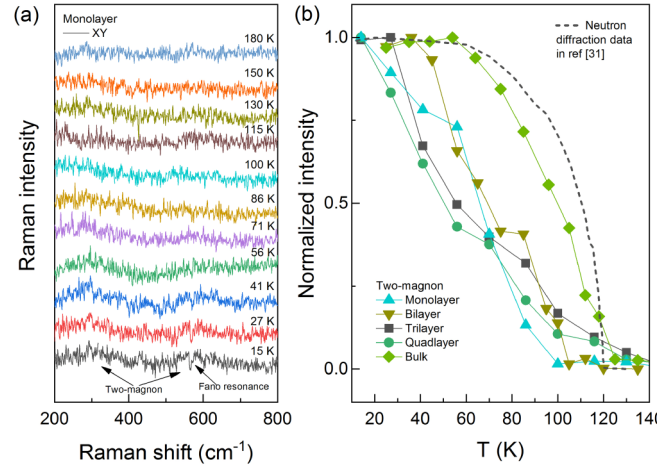

FIG. 4. (a) Raman spectra of monolayer $CoPS_3$ in the range 200–800 cm^{-1} at several representative temperatures in cross-polarization (XY) configuration. Two-magnon peaks are indicated by the black arrows. Fano resonance is also indicated by an arrow. To clearly exhibit two-magnon peaks, the phonon peak P_6 around 250 cm^{-1} is eliminated. (b) Normalized integrated intensity of two-magnon scattering as a function of temperature in $CoPS_3$ with different layer numbers and neutron diffraction data in Ref. [31] as a function of temperature.

~100 K (T_{KT}). On the contrary, the structural transition temperature of few-layered $CoPS_3$ (including monolayer, bilayer, trilayer, and quadlayer) is lower than that of the bulk at 118 K. It suggests that these thin samples have already exhibited 2D behaviors. For the bulk $CoPS_3$, the peak splitting ΔP_2 [red diamonds in Fig. 3(b)] tracks the magnetic scattering intensity in the neutron scattering measurements [short dashed line in Fig. 3(b)], indicting the magnetostriction in the bulk. However, the connection between the structural change and the magnetic transition for few-layered $CoPS_3$ is not established yet. It is our next task to demonstrate it by using two-magnon scattering (Fig. 4), which will be discussed later.

Further evidence for structural distortion due to magnetostriction can be found in the temperature dependence of the peak P_5 near 250 cm^{-1} in monolayer $CoPS_3$. Figure 3(a) shows that the peak energy starts to redshift as temperature decreases below ~85 K [dashed line in Fig. 3(a)], which is near the T_{KT} for thin $CoPS_3$. For bulk samples, the peaks P_5 near 250 cm^{-1} and P_7 near 386 cm^{-1} (green triangles and orange squares in Fig. S6(b) [30]) exhibit a similar temperature-dependent trend as the monolayer one, however, the temperature threshold of the peak energy redshifts and blueshifts is T_N instead of T_{KT}, respectively. Based on the DFT calculations on the vibration modes of the P_5 and P_7, they originate from the out-of-plane vibration of S-S atoms without the participation of any magnetic atom. Therefore, this temperature-dependent Raman shift in monolayer and bulk $CoPS_3$ must be indirectly related to the magnetostrictive effect. We suggest that the distortion of the hexagonal structure formed by Co atoms occuring at low temperature changes the lattice parameters and influences the Raman mode of the $(P_2S_6)^{4-}$ bipyramid structure.

Figure 4(a) shows the temperature dependence of the Raman spectra in the monolayer $CoPS_3$ measured in the cross-polarization (XY) configuration. Because of the suppression of several phonon peaks in this case, it is easier to determine the two-magnon signals and Fano signature. We can clearly observe that the two-magnon signals appear at the central wave number of around 350 and 600 cm^{-1} with an intriguing broad bandwidth at low temperature, which gradually disappears as temperature increases. These observations are the typical phenomena of antiferromagnetic materials, and the similar behaviors can be observed in $NiPS_3$ [37]. Figure 4(b) summarizes the normalized integrated intensities of two-magnon Raman signals as a function of temperature for samples with different thicknesses (the original Raman data are shown in Fig. S8 in the Supplemental Material [30]). For bulk samples, the temperature dependence of the two-magnon Raman is consistent with that of Bragg peak intensity by neutron diffraction measurements in Ref. [31]. As the thickness of samples decreases, the normalized integrated intensities obviously diverge from that of the bulk one. In addition, as shown in Fig. 4(a), the Fano resonance of the P_8 peak can also be observed below 56 K in the cross-polarization (XY) configuration of Raman spectra of the monolayer sample (see Fig. S9 for the zoomed Fano-resonance signal) [30], which gradually rises as the number of layers increases (Fig. S8) [30]. The $1/q$ (see the Supplemental Material for the definition [30]), which represents the strength of coupling between a discrete excitation and a two-magnon excitation, is extracted to be around 0.7 for the bulk material below T_N. As shown in Fig. S10 [30], the coupling strength of the Fano resonance dramatically increases in comparison with

the values above T_N due to the presence of antiferromagnetic orders. Therefore, we establish the connection between the structural change and the magnetic transition for monolayer $CoPS_3$, indicating that the peak splitting in Figs. 2 and 3 is an indicator of the magnetic transition.

For the few layers of $CoPS_3$, the system is described by the two-dimensional XY model and undergoes a finite temperature transition at T_{KT}. Due to the strong magnetostriction effect, the onset of the magnetic order is accompanied by the peak splitting of the phonon modes at around 149 (P_2) cm^{-1}. We expect that the lattice distortion and hence the peak splitting is proportional to the average amplitude of the spin pair $\sum_{\langle ij\rangle}\langle S_i \cdot S_j\rangle$. Although the staggered magnetization is zero, $\langle|S_i|\rangle = 0$, for the monolayer $CoPS_3$, the in-plane correlation length goes to an unusual exponential divergence as T approaches T_{KT} [38], $\xi(T) \sim \exp[B(T/T_{KT}-1)^{-1/2}]$ with $B \sim \pi/2$. Such a divergent correlation length gives rise to the nonzero summation in the spin pair $\sum_{\langle ij\rangle}\langle S_i \cdot S_j\rangle$, resulting in the peak splitting of the phonon modes. We notice that the transition temperature remains unchanged from the monolayer to quadlayer one, indicating the two-dimensional behavior in the few-layered samples.

For the bulk material, the small interlayer coupling of the system slightly modifies the transition temperature, $T_N = T_{KT} + C/[\ln(J'/J)]^2 T_{KT}$ [39], where $C \sim 2$ and J'/J is the ratio between the interlayer and intralayer interactions. As $T_{KT} =$ 100 K for thin samples and $T_N = 118$ K for bulk in the measurements, we can estimate $J'/J = 0.03$. For the bulk case, a 2D XY-like behavior is expected in the temperature range between T_{KT} and T_N, when the 3D fluctuation is weak. Below T_{KT} [green region in Fig. 3(b)], the system is characterized as the quasi-long-range magnetic orders, while it is the paramagnetic state above T_N [purple region in Fig. 3(b)]. Between them [orange region in Fig. 3(b)], the interlayer interaction (J') becomes important for bulk materials, indicating the 3D fluctuations in this regime. Moreover, the effect of the creation of the vortex-antivortex pairs leads a very rapid decrease of the intensity in the neutron scattering and two-magnon Raman scattering as observed in the experiments. The matrix element of the two-magnon Raman scattering is also proportional to $\sum_{\langle ij\rangle}\langle S_i \cdot S_j\rangle$, accounting for the same two-magnon intensity onset temperature as T_{KT} instead of T_N.

IV. CONCLUSIONS

In conclusion, we have successfully demonstrated the paramagnetic-antiferromagnetic phase transition in monolayer $CoPS_3$ with the polarization-resolved Raman spectroscopy. The splitting of the double-degenerate E_g phonon mode of Co-atom related vibration and the appearance of new peaks (P_2') in LL configuration at low temperature clearly indicate the magnetostrictive effect in the presence of quasi-long-range ordering below T_{KT} in a 2D XY-type antiferromagnet. Our results will be helpful in understanding the underlying mechanism of magnetostrictive effect in 2D materials and clearing some obstacles for manufacturing future antiferromagnetic storage devices.

ACKNOWLEDGMENTS

We would like to thank Prof. A. R. Wildes from Institut Laue-Langevin and Prof. H. Lu from SUSTech for helpful discussions. J.F. acknowledges the support from the National Natural Science Foundation of China (Grant No. 11974159) and the Guangdong Natural Science Foundation (Grant No. 2021A1515012316). J.W.M. was partially supported by the program for Guangdong Introducing Innovative and Entrepreneurial Teams (Grant No. 2017ZT07C062), Guangdong Basic and Applied Basic Research Foundation(Grant No. 2020B1515120100, and Shenzhen Key Laboratory of Advanced Quantum Functional Materials and Devices (Grant No. ZDSYS20190902092905285). J.L. acknowledges the support from National Natural Science Foundation of China (Grant No. 11974156) and the Guangdong International Science Collaboration Project (Grant No. 2019A050510001).

The authors declare no conflict of interest.

[1] C. Gong, L. Li, Z. Li, H. Ji, A. Stern, Y. Xia, T. Cao, W. Bao, C. Wang, Y. Wang, Z. Q. Qiu, R. J. Cava, S. G. Louie, J. Xia, and X. Zhang, Discovery of intrinsic ferromagnetism in two-dimensional van der Waals crystals, Nature (London) **546**, 265 (2017).

[2] B. Huang, G. Clark, E. Navarro-Moratalla, D. R. Klein, R. Cheng, K. L. Seyler, D. Zhong, E. Schmidgall, M. A. McGuire, D. H. Cobden, W. Yao, D. Xiao, P. Jarillo-Herrero, and X. Xu, Layer-dependent ferromagnetism in a van der Waals crystal down to the monolayer limit, Nature (London) **546**, 270 (2017).

[3] Y. Deng, Y. Yu, Y. Song, J. Zhang, N. Z. Wang, Z. Sun, Y. Yi, Y. Z. Wu, S. Wu, J. Zhu, J. Wang, X. H. Chen, and Y. Zhang, Gate-tunable room-temperature ferromagnetism in two-dimensional Fe_3GeTe_2, Nature (London) **563**, 94 (2018).

[4] M. Bonilla, S. Kolekar, Y. Ma, H. C. Diaz, V. Kalappattil, R. Das, T. Eggers, H. R. Gutierrez, M.-H. Phan, and M. Batzill, Strong room-temperature ferromagnetism in VSe_2 monolayers on van der Waals substrates, Nat. Nanotechnol. **13**, 289 (2018).

[5] S. Jiang, L. Li, Z. Wang, K. F. Mak, and J. Shan, Controlling magnetism in 2D CrI_3 by electrostatic doping, Nat. Nanotechnol. **13**, 549 (2018).

[6] B. Huang, G. Clark, D. R. Klein, D. MacNeill, E. Navarro-Moratalla, K. L. Seyler, N. Wilson, M. A. McGuire, D. H. Cobden, D. Xiao, W. Yao, P. Jarillo-Herrero, and X. Xu, Electrical control of 2D magnetism in bilayer CrI_3, Nat. Nanotechnol. **13**, 544 (2018).

[7] S. Jiang, J. Shan, and K. F. Mak, Electric-field switching of two-dimensional van der Waals magnets, Nat. Mater. **17**, 406 (2018).

[8] T. Song, X. Cai, M. W.-Y. Tu, X. Zhang, B. Huang, N. P. Wilson, K. L. Seyler, L. Zhu, T. Taniguchi, K. Watanabe, M. A. McGuire, D. H. Cobden, D. Xiao, W. Yao, and X. Xu, Giant tunneling magnetoresistance in spin-filter van der Waals heterostructures, Science **360**, 1214 (2018).

[9] T. Song, Z. Fei, M. Yankowitz, Z. Lin, Q. Jiang, K. Hwangbo, Q. Zhang, B. Sun, T. Taniguchi, K. Watanabe, M. A. McGuire, D. Graf, T. Cao, J.-H. Chu, D. H. Cobden, C. R. Dean, D. Xiao, and X. Xu, Switching 2D magnetic states via pressure tuning of layer stacking, Nat. Mater. **18**, 1298 (2019).

[10] Z. Wang, T. Zhang, M. Ding, B. Dong, Y. Li, M. Chen, X. Li, J. Huang, H. Wang, X. Zhao, Y. Li, D. Li, C. Jia, L. Sun, H. Guo, Y. Ye, D. Sun, Y. Chen, T. Yang, J. Zhang, S. Ono, Z. Han, and Z. Zhang, Electric-field control of magnetism in a few-layered van der Waals ferromagnetic semiconductor, Nat. Nanotechnol. **13**, 554 (2018).

[11] M. Kim, P. Kumaravadivel, J. Birkbeck, W. Kuang, S. G. Xu, D. G. Hopkinson, J. Knolle, P. A. McClarty, A. I. Berdyugin, M. Ben Shalom, R. V. Gorbachev, S. J. Haigh, S. Liu, J. H. Edgar, K. S. Novoselov, I. V. Grigorieva, and A. K. Geim, Micromagnetometry of two-dimensional ferromagnets, Nat. Electron. **2**, 457 (2019).

[12] S. A. Siddiqui, J. Sklenar, K. Kang, M. J. Gilbert, A. Schleife, N. Mason, and A. Hoffmann, Metallic antiferromagnets, J. Appl. Phys. **128**, 040904 (2020).

[13] L. Onsager, Crystal statistics. I. A two-dimensional model with an order-disorder transition, Phys. Rev. **65**, 117 (1944).

[14] N. D. Mermin and H. Wagner, Absence of Ferromagnetism or Antiferromagnetism in One- or Two-Dimensional Isotropic Heisenberg Models, Phys. Rev. Lett. **17**, 1133 (1966).

[15] S. Coleman, There are no Goldstone bosons in two dimensions, Commun. Math. Phys. **31**, 259 (1973).

[16] J. M. Kosterlitz and D. J. Thouless, Ordering, metastability and phase transitions in two-dimensional systems, J. Phys. C: Solid State Phys. **6**, 1181 (1973).

[17] J.-U. Lee, S. Lee, J. H. Ryoo, S. Kang, T. Y. Kim, P. Kim, C.-H. Park, J.-G. Park, and H. Cheong, Ising-Type magnetic ordering in atomically thin $FePS_3$, Nano Lett. **16**, 7433 (2016).

[18] H. Chu, C. J. Roh, J. O. Island, C. Li, S. Lee, J. Chen, J.-G. Park, A. F. Young, J. S. Lee, and D. Hsieh, Linear Magnetoelectric Phase in Ultrathin $MnPS_3$ Probed by Optical Second Harmonic Generation, Phys. Rev. Lett. **124**, 027601 (2020).

[19] Y.-J. Sun, Q.-H. Tan, X.-L. Liu, Y.-F. Gao, and J. Zhang, Probing the magnetic ordering of antiferromagnetic $MnPS_3$ by raman spectroscopy, J. Phys. Chem. Lett. **10**, 3087 (2019).

[20] P. A. Joy and S. Vasudevan, Magnetism in the layered transition-metal thiophosphates MPS_3 (M = Mn, Fe, and Ni), Phys. Rev. B **46**, 5425 (1992).

[21] D. Lançon, H. C. Walker, E. Ressouche, B. Ouladdiaf, K. C. Rule, G. J. McIntyre, T. J. Hicks, H. M. Rønnow, and A. R. Wildes, Magnetic structure and magnon dynamics of the quasi-two-dimensional antiferromagnet $FePS_3$, Phys. Rev. B **94**, 214407 (2016).

[22] A. R. Wildes, K. C. Rule, R. I. Bewley, M. Enderle, and T. J. Hicks, The magnon dynamics and spin exchange parameters of $FePS_3$, J. Phys.: Condens. Matter **24**, 416004 (2012).

[23] D. Lançon, R. A. Ewings, T. Guidi, F. Formisano, and A. R. Wildes, Magnetic exchange parameters and anisotropy of the quasi-two-dimensional antiferromagnet $NiPS_3$, Phys. Rev. B **98**, 134414 (2018).

[24] A. R. Wildes, B. Roessli, B. Lebech, and K. W. Godfrey, Spin waves and the critical behaviour of the magnetization in $MnPS_3$, J. Phys.: Condens. Matter **10**, 6417 (1998).

[25] C. Kim, J. Jeong, P. Park, T. Masuda, S. Asai, S. Itoh, H.-S. Kim, A. Wildes, and J.-G. Park, Spin waves in the two-dimensional honeycomb lattice XXZ-type van der Waals antiferromagnet $CoPS_3$, Phys. Rev. B **102**, 184429 (2020).

[26] J. P. Joule, XVII. On the effects of magnetism upon the dimensions of iron and steel bars, Philos. Mag. (1798-1977) **30**, 76 (2009).

[27] S. Jiang, H. Xie, J. Shan, and K. F. Mak, Exchange magnetostriction in two-dimensional antiferromagnets, Nat. Mater. **19**, 1295 (2020).

[28] C. Murayama, M. Okabe, D. Urushihara, T. Asaka, K. Fukuda, M. Isobe, K. Yamamoto, and Y. Matsushita, Crystallographic features related to a van der Waals coupling in the layered chalcogenide $FePS_3$, J. Appl. Phys. **120**, 142114 (2016).

[29] P. Jernberg, S. Bjarman, and R. Wäppling, $FePS_3$: A first-order phase transition in a "2D" Ising antiferromagnet, J. Magn. Magn. Mater. **46**, 178 (1984).

[30] See Supplemental Material at http://link.aps.org/supplemental/10.1103/PhysRevB.103.235411 for sample growth and characteristics, sample thickness, Raman characteristics, polarization-resolved Raman spectroscopy, and Raman results. It also includes Refs. [31] and [40–46].

[31] A. R. Wildes, V. Simonet, E. Ressouche, R. Ballou, and G. J. McIntyre, The magnetic properties and structure of the quasi-two-dimensional antiferromagnet $CoPS_3$, J. Phys.: Condens. Matter **29**, 455801 (2017).

[32] H. Zeng, J. Dai, W. Yao, D. Xiao, and X. Cui, Valley polarization in MoS_2 monolayers by optical pumping, Nat. Nanotechnol. **7**, 490 (2012).

[33] C. Lee, H. Yan, L. E. Brus, T. F. Heinz, J. Hone, and S. Ryu, Anomalous lattice vibrations of single- and few-layer MoS_2, ACS Nano **4**, 2695 (2010).

[34] T. Li, S. Jiang, N. Sivadas, Z. Wang, Y. Xu, D. Weber, J. E. Goldberger, K. Watanabe, T. Taniguchi, C. J. Fennie, K. F. Mak, and J. Shan, Pressure-controlled interlayer magnetism in atomically thin CrI_3, Nat. Mater. **18**, 1303 (2019).

[35] T. M. G. Mohiuddin, A. Lombardo, R. R. Nair, A. Bonetti, G. Savini, R. Jalil, N. Bonini, D. M. Basko, C. Galiotis, N. Marzari, K. S. Novoselov, A. K. Geim, and A. C. Ferrari, Uniaxial strain in graphene by Raman spectroscopy: *G* peak splitting, Gruneisen parameters, and sample orientation, Phys. Rev. B **79**, 205433 (2009).

[36] C. C. Mayorga-Martinez, Z. Sofer, D. Sedmidubský, Š. Huber, A. Y. S. Eng, and M. Pumera, Layered metal thiophosphite materials: magnetic, electrochemical, and electronic properties, ACS Appl. Mater. Interfaces **9**, 12563 (2017).

[37] K. Kim, S. Y. Lim, J.-U. Lee, S. Lee, T. Y. Kim, K. Park, G. S. Jeon, C.-H. Park, J.-G. Park, and H. Cheong, Suppression of magnetic ordering in XXZ-type antiferromagnetic monolayer $NiPS_3$, Nat. Commun. **10**, 345 (2019).

[38] P. M. Chaikin and T. C. Lubensky, *Principles of Condensed Matter Physics* (Cambridge University Press, Cambridge, UK, 1995).

[39] S. Hikami and T. Tsuneto, Phase transition of quasi-two dimensional planar system, Prog. Theor. Phys. **63**, 387 (1980).

[40] J. Zhang, R. Cui, X. A. Li, X. Liu, and W. Huang, A nanohybrid consisting of $NiPS_3$ nanoparticles coupled with defective graphene as a pH-universal electrocatalyst for efficient hydrogen evolution, J. Mater. Chem. A **5**, 23536 (2017).

[41] M. A. van Veenendaal and G. A. Sawatzky, Nonlocal Screening Effects in 2p x-Ray Photoemission Spectroscopy Core-Level Line Shapes of Transition Metal Compounds, Phys. Rev. Lett. **70**, 2459 (1993).

[42] N. M. Latiff, C. C. Mayorga-Martinez, B. Khezri, K. Szokolova, Z. Sofer, A. C. Fisher, and M. Pumera, Cytotoxicity of layered metal phosphorus chalcogenides (MPXY) nanoflakes; $FePS_3$, $CoPS_3$, $NiPS_3$, FlatChem. **12**, 1 (2018).

[43] I. Kimchi, A. Nahum, and T. Senthil, Valence Bonds in Random Quantum Magnets: Theory and Application to $YbMgGaO_4$, Phys. Rev. X **8**, 031028 (2018).

[44] S. Y. Kim, T. Y. Kim, L. J. Sandilands, S. Sinn, M.-C. Lee, J. Son, S. Lee, K.-Y. Choi, W. Kim, B.-G. Park, C. Jeon, H.-D. Kim, C.-H. Park, J.-G. Park, S. J. Moon, and T. W. Noh, Charge-Spin Correlation in van der Waals Antiferromagnet $NiPS_3$, Phys. Rev. Lett. **120**, 136402 (2018).

[45] D. Gonbeau, T. Coradin, and R. Clement, XPS Study of Stilbazolium Chromophores and Their Intercalation Compounds in the $MnPS_3$ Layered Phase, J. Phys. Chem. B **103**, 3545 (1999).

[46] R. N. Bhatt and P. A. Lee, Scaling Studies of Highly Disordered Spin-$\frac{1}{2}$ Antiferromagnetic Systems, Phys. Rev. Lett. **48**, 344 (1982).